NASA TECHNICAL MEMORANDUM

NASA TM X-1648

NASA TM X-1648

GPO PRICE $ _____

CSFTI PRICE(S) $ _____

Hard copy (HC) 3.00

Microfiche (MF) .65

ff 653 July 65

EX[redacted]A

T[redacted]

SU[redacted]X'

A[redacted]A

by[redacted]*ip*

Le[redacted]

Cl[redacted]

NAT[redacted]SH

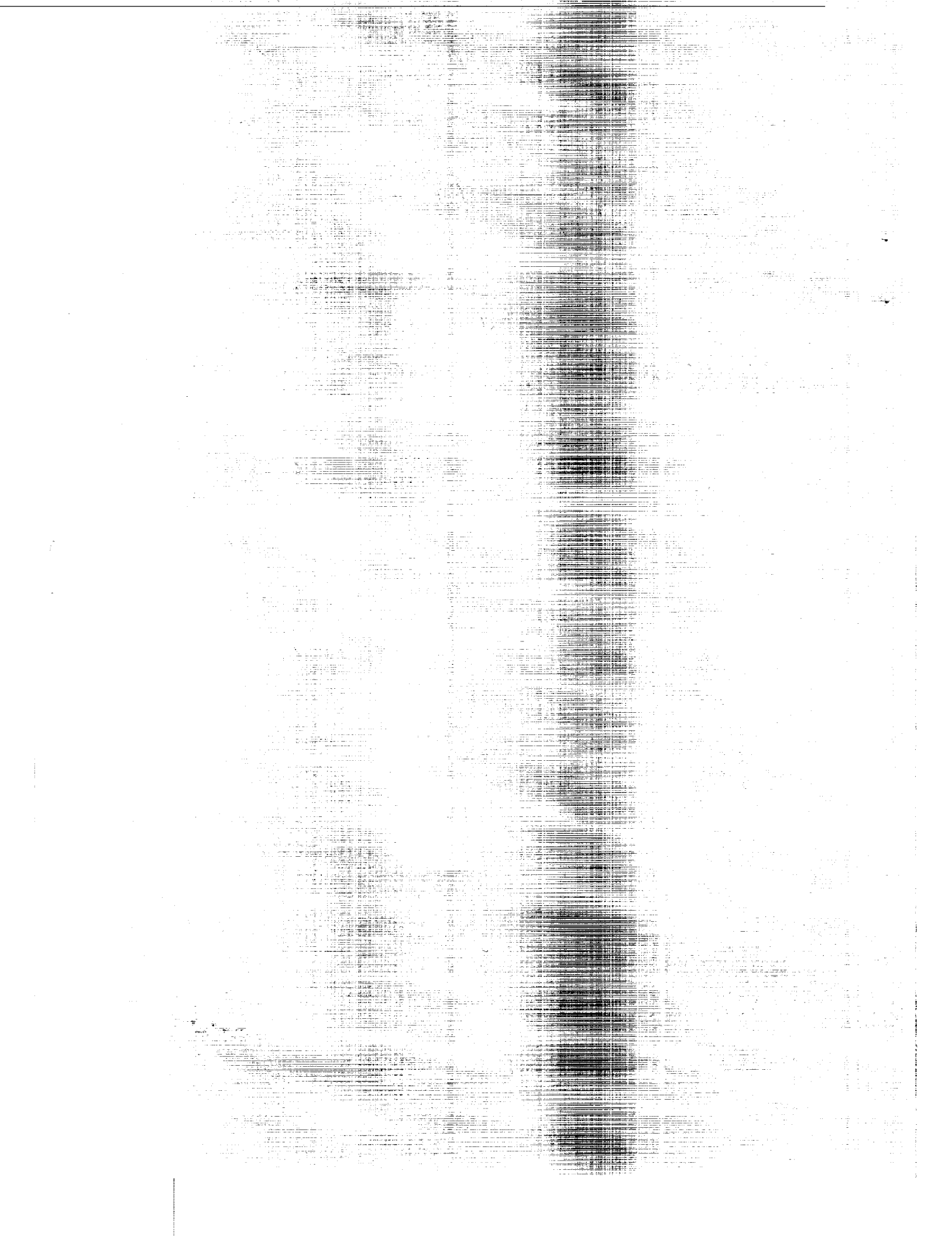

NASA TM X-1648

EXPERIMENTAL INVESTIGATION OF THE DYNAMIC RESPONSE OF A SUPERSONIC INLET TO EXTERNAL AND INTERNAL DISTURBANCES

By Joseph F. Wasserbauer and Daniel L. Whipple

Lewis Research Center
Cleveland, Ohio

NATIONAL AERONAUTICS AND SPACE ADMINISTRATION

For sale by the Clearinghouse for Federal Scientific and Technical Information
Springfield, Virginia 22151 – CFSTI price $3.00

ABSTRACT

The terminal shock position and static-pressure responses of an inlet were measured at a Mach number of 3.0 in the 10- by 10-Foot Supersonic Wind Tunnel. Internal and external disturbances were investigated over frequency ranges of 0.3 to 200 and 0.1 to 12 Hz, respectively. For an internal disturbance, the dynamic response of the terminal shock and static pressure near the inlet throat exhibited a lag characteristic to about 40 Hz but encountered resonant conditions at about 85 and 180 Hz. For the external disturbance, the dynamic response of the terminal shock and static pressure near the inlet throat exhibited a lead characteristic.

EXPERIMENTAL INVESTIGATION OF THE DYNAMIC RESPONSE OF A SUPERSONIC INLET TO EXTERNAL AND INTERNAL DISTURBANCES

by Joseph F. Wasserbauer and Daniel L. Whipple

Lewis Research Center

SUMMARY

The dynamic response of the terminal shock position and of static pressures in the subsonic diffuser of an axisymmetric external-internal-compression inlet were measured at a Mach number of 3.0 in the 10- by 10-Foot Supersonic Wind Tunnel. Internal and external disturbances were investigated over frequency ranges of 0.3 to 200 and 0.1 to 12 hertz, respectively. For an internal disturbance, the dynamic response of the terminal shock and static pressure near the inlet throat exhibited a lag characteristic to about 40 hertz but encountered resonant conditions at about 85 and 180 hertz. These resonances are characteristic of a distributed parameter system. For the external disturbance, the dynamic response of the terminal shock and static pressure near the inlet throat exhibited a lead characteristic.

INTRODUCTION

For optimum inlet performance to be achieved, the inlet control for a mixed-compression inlet must maintain the terminal shock as near to the inlet aerodynamic throat as possible without incurring an unstart. To design the inlet control system properly requires knowledge of the inlet dynamic characteristics; in particular, the dynamic response of the terminal shock position to both internal and external disturbances must be established. An analysis in reference 1 predicts a first-order lag relation between shock position and small downstream pressure disturbances that occur at frequencies below a certain limit. Experimental data on the dynamics of supersonic inlets (refs. 2 and 3) indicate that they act as first-order lag systems with dead time and are in agreement with a Lumped Parameter analysis (refs. 4 to 6). However, the experimental results for mixed-compression and external-compression inlets have been, in general, limited to internal disturbance frequencies less than 50 hertz (refs. 2 to 5 and 7 to 9).

Further insight into the dynamic characteristics of supersonic inlets can be obtained if disturbance frequencies greater than those already investigated are used. In the present investigation, internal disturbance frequencies up to 200 hertz were generated by a rotating bypass valve whose exit area varied in a sinsoidal manner. This choked area disturbance is useful because (a) it is well defined, (b) it is also a sinsoidal flow disturbance, (c) real disturbances might be of this nature, and (d) control loops are closed through bypass area devices. A "gust generator" plate positioned ahead of the inlet was sinusoidally varied to frequencies of 12 hertz to obtain the dynamic response of the inlet to an external disturbance.

Methods for experimentally determining the dynamics of the terminal shock are presented and compared. Amplitude ratio and phase shift are presented for all pressure transducer data and also for the shock-position dynamics. The designs of the rotating bypass valve and the gust plate are also described.

SYMBOLS

A	area, m^2
A_i	projected inlet area, 0.166 m^2
B	constant, cm
f	frequency, Hz
L	length, cm
m	mass flow, kg/sec
n	integer, $n \geq 2$
P	total pressure, N/m^2
P_0	free-stream total pressure, 1.52×10^5 N/m^2
p	static pressure, N/m^2
r	radius of rotating plate, cm
T_0	free-stream total temperature, 382 K
t	time, sec
x	linear distance, cm
α	gust-plate angle of attack, deg
θ	angle, rad
φ	phase shift, deg

ω rotational rate, rad/sec.

Subscripts:

d subsonic diffuser

e valve exit station

i inlet lip station

0 free-stream conditions

APPARATUS AND PROCEDURE

The investigation was conducted in the 10- by 10-Foot Supersonic Wind Tunnel at a free-stream Mach number of 3.0 and a Reynolds number of 0.762×10^6 per meter. A schematic diagram of the inlet cold-pipe configuration used herein is presented in figure 1 and indicates the locations of the pressure transducers and the sinusoidal bypass-valve apparatus. A description of the inlet is given in reference 10. The inlet, designed for operation at Mach number 3.0, had an isentropic spike that compressed the flow to an average Mach number of 2.37 at the cowl lip station. Further internal supersonic compression reduced the Mach number to an average of 1.45 ahead of the terminal shock. A slight modification was made in the diffuser area in the throat region of the inlet from that reported in reference 10. The resulting area variation of the inlet is shown in figure 2. The area of the duct downstream of the diffuser exit station to the model exit plug remained constant.

The internal disturbance was generated by the bypassing of a portion of the internal flow just downstream of the compressor face station through a rotating bypass valve whose exit area varied sinusoidally. The rotating valve and its adaptation to the model are shown in the schematic drawing of figure 3. The valve location on the model is shown in figures 1(a) and (c). The flow through the valve was choked at all times. The valve was driven by a hydraulic motor, the flow through which was varied to control the speed. Two hydraulic motors of different speed ranges were used to obtain frequencies that ranged from about 0.3 to as high as 200 hertz. Closing off one exit port could reduce the variation in the rotary-valve-exit area by one-half. A rotary-variable-differential transformer (RVDT) was used to record the position and frequency of the rotating valve. The RVDT was calibrated to allow correction of the valve-position signal because the RVDT introduced a phase shift at the higher frequencies. The equation describing the valve rotor contour and the derivation of the valve-exit-area variation is presented in the appendix. For data taking, the desired disturbance frequency was set with a hydraulic flow regulator; then the valve-position signal and pressure disturbance data were recorded on magnetic tape.

The external disturbance was generated by a large trapezoidal gust plate mounted in the tunnel just upstream of the inlet, as shown in the schematic drawing of figure 4. The gust plate was oscillated about a fixed pivot. A linear potentiometer provided position information for the control room readout as well as the position feedback for the control system, which was a simple position-feedback system with a sine-wave oscillator to provide the reference signal. An electrohydraulic servovalve drove the hydraulic cylinder in response to an electrical signal from the control system. A derivation of the gust-plate motion against the hydraulic cylinder motion is given in the appendix. In operation, the disturbance frequency was selected on the function generator, and the gust-plate amplitude was set by observation of the gust-plate oscillation on a light-beam oscillograph (generally $\pm 1/2^{\circ}$ of arc).

The pressure disturbances in the model were sensed with strain-gage-type transducers and recorded on dynamic instrumentation. The tubes leading to the transducers were kept short (approx. 5 cm long) except for the sensor in the bypass-valve duct. This tube was 15.2 centimeters long. The tube-transducer assemblies were calibrated to allow for correction of the pressure fluctuation signals due to tube-assembly dynamics at the higher frequencies. The tube-transducer assemblies had resonant frequencies of 740 and 380 hertz for the 5- and 15.2-centimeter tube lengths, respectively. The corrected data then gave information concerning the dynamic response of inlet duct pressures resulting from both internal and external disturbances.

Prior to the dynamic testing, curves of the inlet steady-state performance were generated for the sinusoidal bypass valve in the closed and open positions (fig. 5). Also shown in figure 5 is the performance of the present inlet with the bypass valve sealed. During operation of the sinusoidal valve, the bypass flow through the valve varied from about 4 to 8 percent of the inlet mass flow. The inlet dynamic response was obtained for two inlet conditions corresponding to exit-plug corrected air flow of 10.5 and 10.7 kilograms per second (fig. 5). The duct Mach numbers just upstream of the exit plug for these two conditions were recorded as 0.304 and 0.308, respectively. These two inlet conditions are termed as near critical and supercritical operation, respectively. Figure 6 shows the effect of valve position on the steady-state internal-cowl pressure distributions for the exit-plug position corresponding to near-critical operation. For this position, the terminal shock travel was centered on the four transducers (A, B, C, and D) located in the inlet throat.

The shock-position amplitude for all frequencies was determined from the analog signals of these four throat transducers and analyzed as shown in figure 7. The sinusoidal bypass-valve position is also shown in the figure. As the shock moves across each transducer, a sharp rise and fall in pressure is recorded. If the time of these sharp increases and decreases is plotted against the transducer position, a graph of shock position against time can be constructed. The method of least squares

was used to fit a sinewave to shock-position data. Amplitude and phase shift could then be determined for shock-position dynamics.

Another method used to determine shock-position dynamics was the inlet unstart method. In this method, an equivalent shock travel was obtained at each valve frequency f from the corresponding unstart plug position u_f. For this inlet, the terminal shock position was a linear function of the choked exit area of either the plug or the rotary valve. In addition, the plug area was a linear function of plug position in the region of interest. Therefore, an equivalent terminal shock oscillation amplitude ratio could be obtained from the unstart plug positions u_f at different valve frequencies.

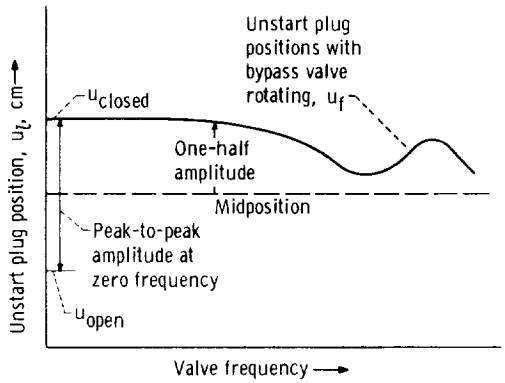

The above sketch presents the variation of unstart plug position u_f as rotary valve frequency is varied. A normalizing amplitude is obtained by determining the plug travel equivalent to the rotary valve area disturbance, which is, in turn, proportional to the peak-to-peak terminal shock movement. This equivalent plug travel is obtained from the unstart plug positions for the rotary valve open and closed (u_{open} and u_{closed}). To determine the unstart plug position at a valve frequency f, the plug is closed slowly with respect to the valve rotation. Therefore, at very low valve frequencies, the inlet will unstart when the valve passes the closed position so that $u_f = u_{closed}$. At higher frequencies, if the terminal shock did not respond to the rotary valve disturbance, the unstart plug position u_f would be midway between the u_{open} and u_{closed} positions. This is because the rotary valve flow would be an average of the open and closed valve flows. The unstart plug positions will therefore be restricted to values above the plug midposition (indicated in the sketch), which permits measurement of only one-half the amplitude. Therefore, from these considerations, an equivalent terminal shock amplitude ratio can be obtained from the corresponding unstart plug position by the following relation:

$$\text{Amplitude ratio} = \frac{2u_f - (u_{closed} + u_{open})}{u_{closed} - u_{open}}$$

In this method, the terminal shock does not oscillate about the same mean position when the amplitude is determined at different valve frequencies, and no phase information is obtained. However, as long as the linear relation between shock and plug positions is valid, the method provides easily reduced data. In addition, the method has no characteristics that would impose a frequency limit on its use.

The dynamic responses of the pressures at the various inlet stations were measured from oscillograph traces. An average value of amplitude and phase shift for each pressure was determined from readings taken over several cycles of valve rotation at constant frequency.

All data presented in the succeeding figures are in terms of amplitude ratio and phase shift. The amplitude ratio is defined as the signal amplitude at the test frequency divided by the amplitude at zero frequency. The amplitude for zero frequency was assumed to be the same as the amplitude recorded at a frequency of 1 hertz or less for the shock position and the static-pressure responses.

RESULTS AND DISCUSSION

Internal Disturbance Dynamics

Figure 8 presents the variation with frequency of the terminal-shock-position amplitude ratio as obtained by the inlet unstart method. The experimental data indicate that resonances in the amplitude ratio occur at about 85 and 180 hertz. The amplitude of the first resonance is one-half the amplitude observed at a frequency of 1 hertz or less. Previous studies on inlet dynamics have not shown any resonant conditions in their dynamic response, possibly because of the limitation on the disturbance frequency. The disturbance amplitude (rotary-valve-total-exit area) was reduced one-half by sealing one exit port, and the results are also shown in figure 8. Little or no variation in the inlet shock-position dynamics was observed at the reduced disturbance amplitude. Therefore, throughout the remainder of the report, only data obtained with the full-amplitude disturbance are presented.

Figure 9(a) shows the shock-position amplitude ratio and the phase shift variation with frequency for the data reduction method described in figure 7. The data presented in this figure confirm the resonance condition observed from the inlet unstart method. The scatter in the data is a direct result of the limited instrumentation in the throat region of the inlet. The accuracy of the curve fitting by the method of the least

squares is reduced when less than eight data points per cycle are obtained. For some of the low-amplitude data at a higher frequency, only three to four points per cycle were obtained. Data are not presented above 100 hertz because of the reduced definition in the transducer signals.

Figure 9(b) presents the phase shift associated with the shock-position dynamics. In general, the phase shift shows an increasing lag with increasing frequency until a frequency of 20 to 30 hertz is reached. A lead component in the phase shift is observed from about 30 to 50 hertz, after which a sharp increase in the phase lag is noted. This type of phase shift behavior is characteristic of a resonance condition.

Figure 10 presents the dynamic response of the static pressure just downstream of the inlet throat. This static is located 21.9 centimeters from the cowl lip, as noted in figure 1(b). Here again, the resonant conditions are observed at 85 and 180 hertz (fig. 10(a)). The magnitude of the amplitude ratio at the resonant condition appears to be the same as that determined for the shock-position dynamics. Examination of figure 10(b) shows that the trends observed in phase shift are also similar to those obtained for the shock-position dynamics. The dashed lines in figure 10 are the results for the lumped-parameter analysis of reference 5. The comparison is made only to show that this analysis is limited in its application to the low-frequency range. As indicated by the comparison, the limitations in phase shift appear to be greater than those of the amplitude ratio.

Comparison of figures 10(b) and 9(b) shows that the phase shift for the shock-position dynamics has a larger lag component beyond the first resonance than that for the static pressure just downstream of the throat. Reference 1 indicates that there should be a first-order lag relation between shock position and small downstream disturbances in pressure that occur at frequencies below a given limit. Figure 11 presents the difference between figures 10(b) and 9(b) and is empirically fit with the phase shift of a first-order system whose corner frequency of 50 hertz is similar to that of the experimental data. (The corner frequency of a first-order system is defined as that frequency at which the output lags the input by 45°.) The agreement indicates that the first-order approximation appears reasonable; however, the empirical corner frequency is about 3.6 times the corner frequency predicted by reference 1. The first-order relation is not immediately evident when the amplitude ratios of figure 10(a) are compared with those of 9(a), but it may be present within the scatter of the data.

The dynamic response of a static pressure at the subsonic diffuser exit station is presented in figure 12. This response appears to be similar to the response of the static pressure near the inlet throat (fig. 10), with the exception of the additional resonance at 120 hertz. A possible explanation of why the response here should be different from those observed for the shock-position response and the pressure response just downstream of the shock is that the disturbance is unsymmetrical. Also, the inlet duct is partitioned by two struts that house the centerbody bleed ducts and extend from a model

station of about 50.8 to about 152.4 centimeters (fig. 1(a)). The rotary valve and compressor face transducer were both located in one-half of this duct, as noted in figure 1(c). This particular duct geometry could complicate the dynamic response of pressures at this station and at other locations in the inlet duct because of the varied paths by which the pressure waves can be transmitted.

The phase shift associated with the dynamic response for the pressure at this station is presented in figure 12(b). Here, a near-zero phase shift appears at about 50 hertz with an increasing lag for frequencies greater than 100 hertz.

The dynamic response of the static pressure measured in the bypass duct of the rotary valve assembly is presented in figure 13(a). No predominant resonances were observed in the experimental data; however, a gradual rise in the amplitude ratio is noted for the disturbance frequencies above 100 hertz. The phase shift associated with the dynamic response of this static pressure is presented in figure 13(b). The data presented in figure 13 required the most correction for line dynamics because of the tube length ahead of the transducer.

The data for the dynamic response of the static pressure near the model exit are presented in figure 14. The amplitude ratio at this station (fig. 14(a)) shows a different response from that observed at the compressor face and at the inlet throat region. A resonance is indicated at a frequency of approximately 180 hertz. Also, a damped resonance in the amplitude ratio appears to be present at approximately 50 hertz. Again, the dynamics here could be influenced by the particular duct geometry ahead of this station. The phase shift associated with the dynamics at this station is shown in figure 14(b). A gradual increase in lag is noted to about 10 hertz, after which an apparent lead component in the phase shift is evident. A distinct lead component in the phase shift is evident at about 90 hertz.

The difference in phase lag from the diffuser exit station (fig. 12(b)) to both the throat exit pressure and the model exit pressure stations can be calculated by use of the dead time parameter of reference 4. The dead time is the time required for a pressure wave to travel from a disturbance directly to a pressure-sensing station and is based on the sonic velocity plus or minus the local gas velocity. The dead time calculated for the static pressure at the cowl station of 21.9 centimeters was 0.0036 second, and the dead time for the static at the model exit station was 0.0041 second. Good agreement with the data was obtained when these dead times were applied.

External Disturbance Dynamics

For the external disturbance, data are presented only for the shock-position dynamics and for the static pressure at the cowl station 21.9 centimeters from the cowl lip.

For the internal disturbance the entering flow remains constant in all respects in the supersonic section of the inlet, and only the subsonic portion is affected by the disturbance. However, for the external disturbance, the inlet flow varies with the disturbance in both the supersonic and subsonic portions. In addition to a change in the free-stream Mach number, the disturbance in the external flow includes changes in flow angle of attack.

The dynamic response of the terminal shock resulting from the external disturbance generator is presented in figure 15. These data were obtained with the inlet unstart method. The dynamic response in amplitude ratio indicates a lead system and is just the opposite of that observed for the internal disturbance generator. This difference indicates that an inlet unstart could be caused by a higher-frequency disturbance of the same amplitude as a low-frequency disturbance, which does not cause inlet instart.

Figure 16(a) shows the dynamic response of the terminal shock as obtained by the method outlined in figure 7 for near-critical inlet operation. Both methods for determining shock-position dynamics are in agreement. The phase shift associated with the shock-position dynamics for the external disturbance shows a phase lead (fig. 16(b)). This lead suggests that for external disturbances the inlet dynamics give evidence of at least a first-order lead system at these low-disturbance frequencies.

Figure 17 shows the concurrent dynamic response in amplitude ratio and phase shift for the static pressure just downstream of the inlet throat. The trends in the dynamic response appear to be the same as those observed for the shock position dynamics, except that the magnitude of the amplitude ratio is less than that observed for the terminal shock. No measurable response of the other internal statics was obtained.

Apparent from the experimental results is that the prediction of inlet dynamics at high frequencies cannot be made by the lumped parameter analysis of references 4 to 6. A distributed parameter analysis is also described in reference 6. When the distributed inertia, capacitance, resistance, and terminating impedance are known, such as for the constant-area duct illustrated in reference 6, the predicted dynamic response exhibits repeated resonances as the disturbance frequency is increased. The dynamic response of the pressures throughout the inlet of the present study are characteristic of such a distributed parameter system. Application of this analysis to the present model would be difficult because not only do the inertia, capacitance, and resistance change along the duct, but the impedance also varies. An analysis based on distributed parameters and geometry variation would have to be made for a more accurate prediction; however, such an analysis is beyond the scope of this report.

CONCLUDING REMARKS

An external-internal compression inlet designed for a Mach number of 3.0 was

dynamically tested with both internal and external disturbances. The internal disturbance was generated by a rotating bypass valve positioned just aft of the compressor face station. The valve exit area was varied sinusoidally to frequencies of 200 hertz. The external disturbance was generated by a gust plate that was oscillated sinusoidally to frequencies of 12 hertz. The dynamic responses of both the terminal shock and the static pressures at various stations throughout the model were measured. The following results were obtained:

1. For the inlet dynamics due to an internal disturbance, resonances in the dynamic response of the terminal shock position and of the static pressures in the diffuser were observed experimentally. The resonant conditions occurred at 85 and 180 hertz for the terminal shock position and for static pressures near the inlet throat. Pressure measurements downstream in the inlet duct also indicated resonances but at differing frequencies depending on position.

2. The resonant conditions observed for the dynamic response of pressures throughout the inlet are characteristic of a distributed parameter system.

3. For the external disturbance, the experimentally determined inlet dynamics indicated a leading characteristic for both the terminal shock-position and static-pressure dynamics near the inlet throat over a frequency range of 0.1 to 12 hertz. Therefore, this inlet was more sensitive to higher-frequency external disturbances than was indicated by steady-state measurements.

Lewis Research Center,
National Aeronautics and Space Administration,
Cleveland, Ohio, April 29, 1968,
720-03-01-62-22.

APPENDIX - DISTURBANCE GENERATORS

Internal Disturbance Generator

The desired disturbance device was one that would provide a sinusoidal area variation of constant amplitude over a wide frequency range. Mechanical and electrical simplicity was also desired.

Obtaining a sinusoidally varying area without encountering the inertia limitations associated with an oscillating system required the use of a unidirectional rotating valve. The valve consisted of two plates, one fixed and one rotating at a frequency ω. In general, the fixed plate may have n symmetric wedge-shaped ports, and the rotating plate has an outer radius that varies sinusoidally with n cycles in its circumference. As indicated in the following sketch, the wedge opening is given as $\Delta\theta$, a fixed angle of π/n radians, and the radius of the rotating plate is given by

$$r = R + B \cos n\theta$$

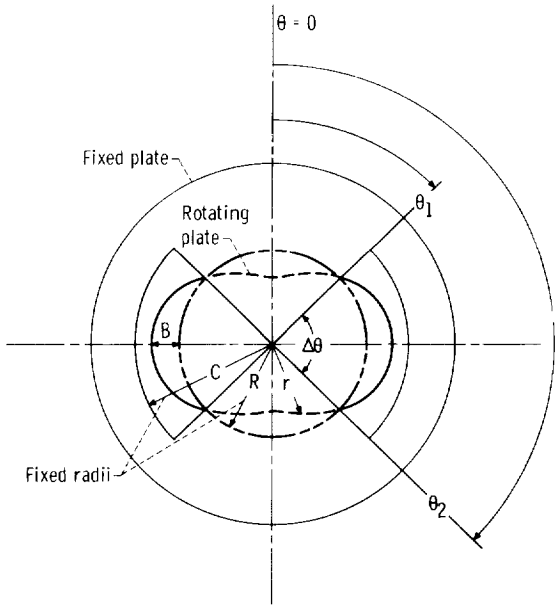

The open area for one segment is given as the port area $\pi C^2/2n$ minus the exposed area of the rotating plate. The exposed area of the rotating plate is given by

$$A = \frac{1}{2}\int_{\theta_1}^{\theta_2} (R + B \cos n\theta)^2 \, d\theta$$

Expanding and grouping terms gives

$$2A = \int_{\theta_1}^{\theta_2} R^2 \, d\theta + \int_{\theta_1}^{\theta_2} 2RB \cos n\theta \, d\theta + \int_{\theta_1}^{\theta_2} B^2 \cos^2 n\theta \, d\theta$$

and integrating yields

$$2A = R^2(\theta_2 - \theta_1) + \frac{2RB}{n}(\sin n\theta_2 - \sin n\theta_1) + \frac{B^2}{2}(\theta_2 - \theta_1) + \frac{B^2}{n}\left[\frac{1}{4}(\sin 2n\theta_2 - \sin 2n\theta_1)\right]$$

Since

$$\theta_2 - \theta_1 = \Delta\theta$$

then

$$\theta_2 = \Delta\theta + \theta_1$$

Substituting for θ_2 and noting that

$$\sin (x + y) = (\sin x)(\cos y) + (\cos x)(\sin y)$$

gives

$$A = \frac{R^2 \, \Delta\theta}{2} + \frac{B^2 \, \Delta\theta}{4} + \frac{RB}{n}(\sin n\theta_1 \cos n \, \Delta\theta + \cos n\theta_1 \sin n \, \Delta\theta - \sin n\theta_1)$$

$$+ \frac{B^2}{8n}(\sin 2n\theta_1 \cos 2n \, \Delta\theta + \cos 2n\theta_1 \sin 2n \, \Delta\theta - \sin 2n\theta_1)$$

Now, if $\Delta\theta$ is constrained to equal $180^{o}/n = \pi/n$ radians and it is noted that

$$\left.\begin{aligned} \cos \pi &= -1 \\ \cos 2\pi &= 1 \\ \sin \pi &= 0 \\ \sin 2\pi &= 0 \end{aligned}\right\}$$

the expression for A reduces to

$$A = \frac{R^2\pi}{2n} + \frac{B^2\pi}{4n} - \frac{2RB}{n} \sin n\theta_1$$

The open area A_e is then defined as

$$A_e = \frac{\pi C^2}{2n} - A$$

$$= \frac{\pi}{2n}\left(C^2 - R^2 - \frac{B^2}{2}\right) + \frac{2RB}{n} \sin n\theta_1$$

For a plate rotation of frequency ω_1, the angle θ_1 varies as

$$\theta_1 = \omega_1 t$$

and because none of the variables in the area integral are time dependent, the change of variables is valid. Letting

$$K = \frac{\pi}{2}\left(C^2 - R^2 - \frac{B^2}{2}\right)$$

gives

$$A_e = \frac{K}{n} + \frac{2RB}{n} \sin n\omega t$$

The total valve area change is nA_e, where the integer $n \geq 2$ in order to obtain a dynamically balanced rotating plate.

The derived area A_e gives a sinusoidal area variation with maximum and minimum areas that can be easily selected and with a frequency that can be determined by any integral multiple (except 1) of the rotation frequency of the moving plate. Therefore, a readily available motor can be used to drive the rotating plate at $1/n$ of the desired disturbance frequency. The amplitude of the exit area can be varied in increments from nA_e to A_e when the wedge-shaped ports are blocked off from 0 to (n - 1).

External Disturbance Generator

A derivation of the gust-plate motion is presented to show that the assumption of sinusoidal motion is valid. From the sketch, m, e, and d are fixed lengths. Let $\theta = \alpha + \delta$ and from the law of cosines,

$$(m + A \sin \omega t)^2 = d^2 + e^2 - 2 de \cos \theta$$

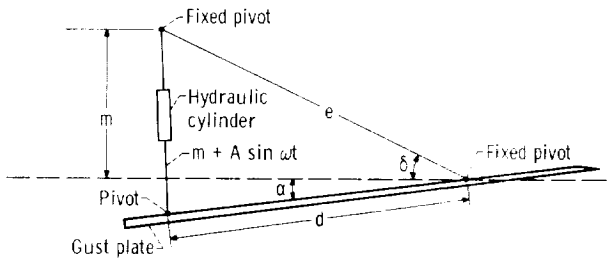

Substituting for θ and expanding give

$$(m + A \sin \omega t)^2 = d^2 + e^2 - 2 de \left[(\cos \alpha)(\cos \delta) - (\sin \alpha)(\sin \delta)\right]$$

Because the hydraulic cylinder actuation arm is normal to the gust plate at $\alpha = 0^o$, then

$$\sin \delta = \frac{m}{e}$$

and

$$\cos \delta = \frac{d}{e}$$

Thus,

$$(m + A \sin \omega t)^2 = d^2 + e^2 - 2 de \left[(\cos \alpha) \frac{d}{e} - (\sin \alpha) \frac{m}{e}\right]$$

$$= d^2 + e^2 - 2d^2 \cos \alpha + 2dm \sin \alpha$$

Now $m^2 + d^2 = e^2$ and α is small, then $\cos \alpha = 1$ and $\sin \alpha = \alpha$. Therefore,

$$(m + A \sin \omega t)^2 = d^2 + e^2 - 2d^2 + 2dm\alpha$$

$$= e^2 - d^2 + 2dm\alpha$$

$$= m^2 + 2dm\alpha$$

Expanding the left side of the equation gives

$$m^2 + 2Am \sin \omega t + A^2 \sin^2 \omega t = m^2 + 2dm\alpha$$

and solving for α yields

$$\alpha = \frac{A}{d} \sin \omega t + \frac{A^2}{2md} \sin^2 \omega t$$

when A is constrained to be $A << 2m$, then

$$\frac{A}{d} >> \frac{A^2}{2md}$$

and from this,

$$\alpha = \frac{A}{d} \sin \omega t \qquad \text{(for small } \alpha\text{)}$$

REFERENCES

1. Hurrell, Herbert G.: Analysis of Shock Motion in Ducts During Disturbances in Downstream Pressure. NACA TN 4090, 1957.

2. Hurrell, Herbert G.: Experimental Investigation of Dynamic Relations in a 48-Inch Ram-Jet Engine. NACA RM E56F28, 1957.

3. Bowditch, David N.; Anderson, Bernhard H.; and Tabata, William K.: Performance and Control of a Full-Scale, Axially Symmetric External-Internal-Compression Inlet from Mach 2.0 to 3.0. NASA TM X-471, 1961.

4. Hurrell, Herbert G.: Simplified Theory for Dynamic Relation of Ramjet Pressures and Fuel Flow. NACA RM E57I13, 1957.

5. Bowditch, David N.; and Wilcox, Fred A.: Dynamic Response of a Supersonic Diffuser to Bypass and Spike Oscillation. NASA TM X-10, 1959.

6. McGregor, W. K., Jr.; Russell, D. W.; Messick, R. W.; and Burns, L. F.: Analysis of Gas Flow Systems for Dynamic Control Purposes. Aro, Inc. (AEDC TR 55-11), Apr. 1956.

7. Anon.: Investigation of Supersonic Transport Engine Inlet Configurations. Rep. LR-19014, Lockheed Aircraft Co. (NASA CR-68399), Sept. 30, 1965.

8. Martin, Arnold W.; and Kostin, Leonard C.: Propulsion System Dynamic Test Results. Rep. NA-67-386, North American Aviation, Inc. (NASA CR-73114), Apr. 17, 1967.

9. Chun, K. S.; and Swanson, D. R.: Dynamic Simulation of Supersonic Inlet and Engine. Paper No. 64-598, AIAA, Aug. 1964.

10. Stitt, Leonard E.; and Salmi, Reino J.: Performance of a Mach 3.0 External-Internal-Compression Axisymmetric Inlet at Mach Numbers from 2.0 to 3.5. NASA TM X-145, 1960.

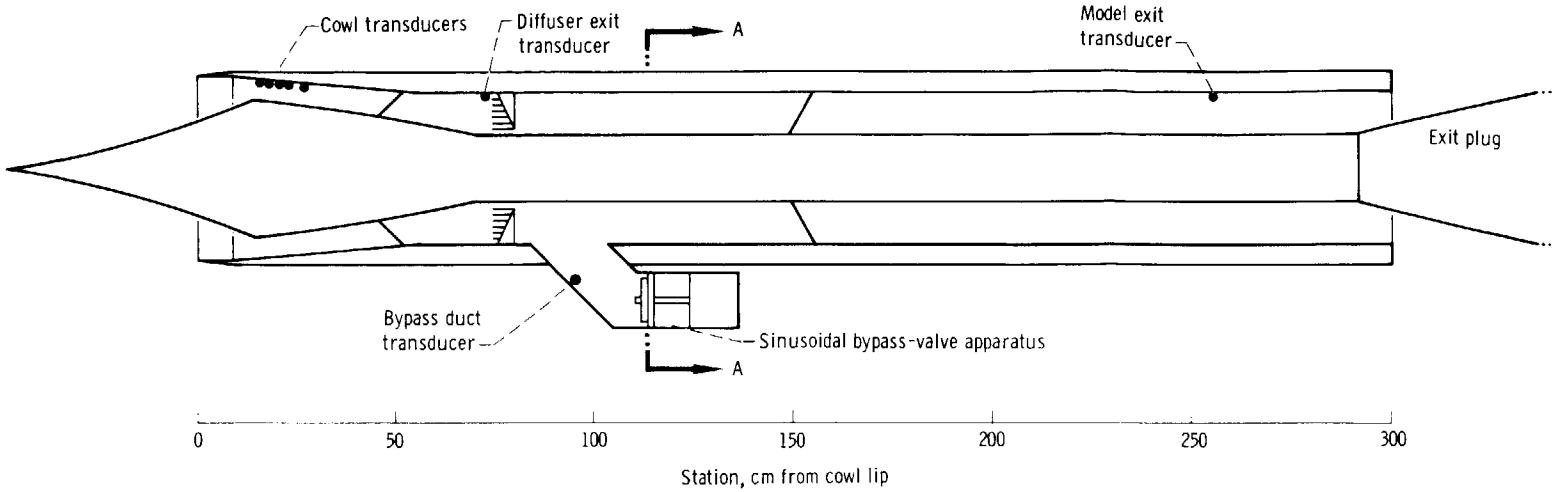

(a) Test configuration.

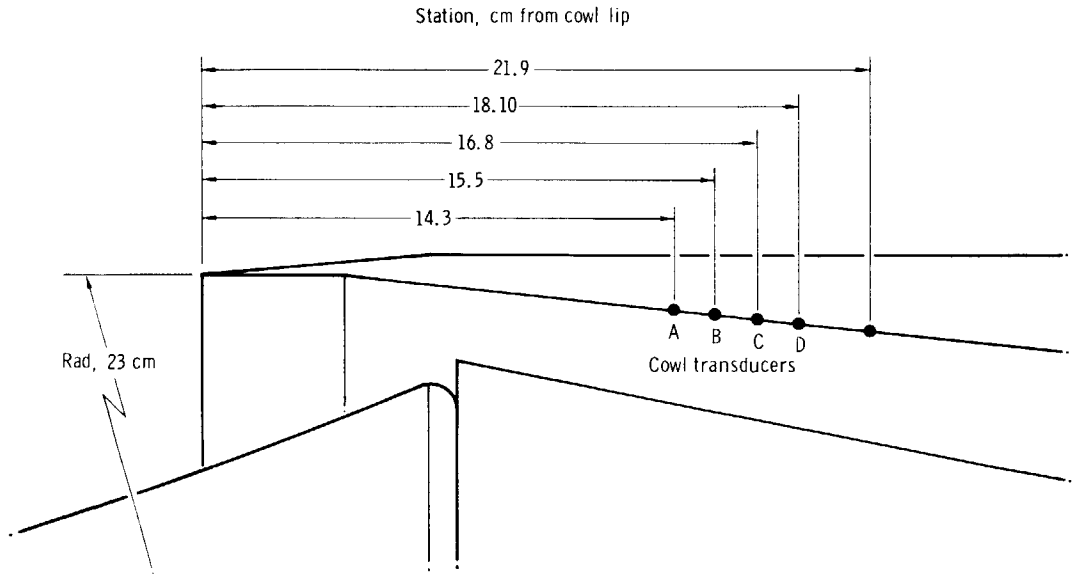

(b) Enlarged view of shock-position transducers location.

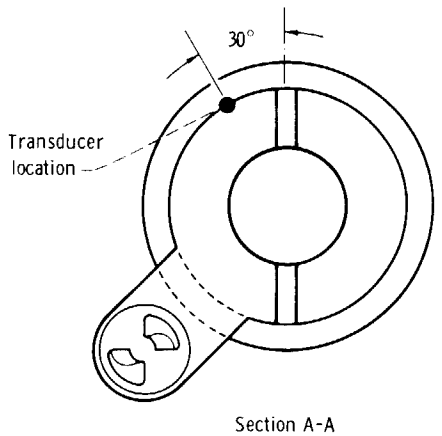

CD-9822-01

(c) Sinusoidal bypass-valve station.

Figure 1.- Sinusoidal bypass-valve test configuration and transducer locations.

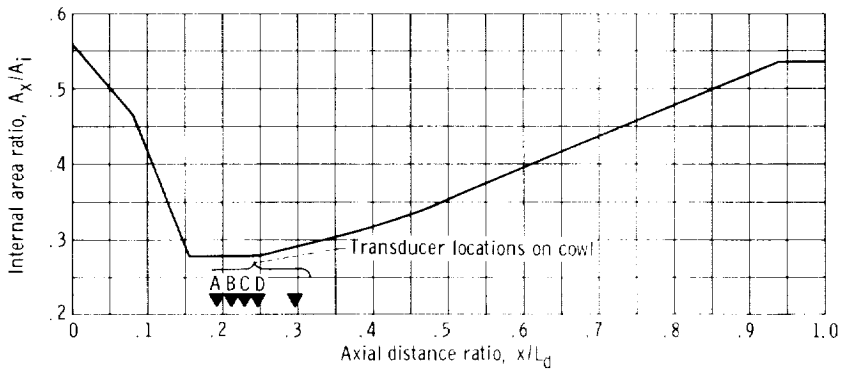

Figure 2. - Variation of diffuser internal area ratio. Subsonic diffuser length, 73.7 centimeters; axial distance ratio, 0 (corresponds to cowl lip station).

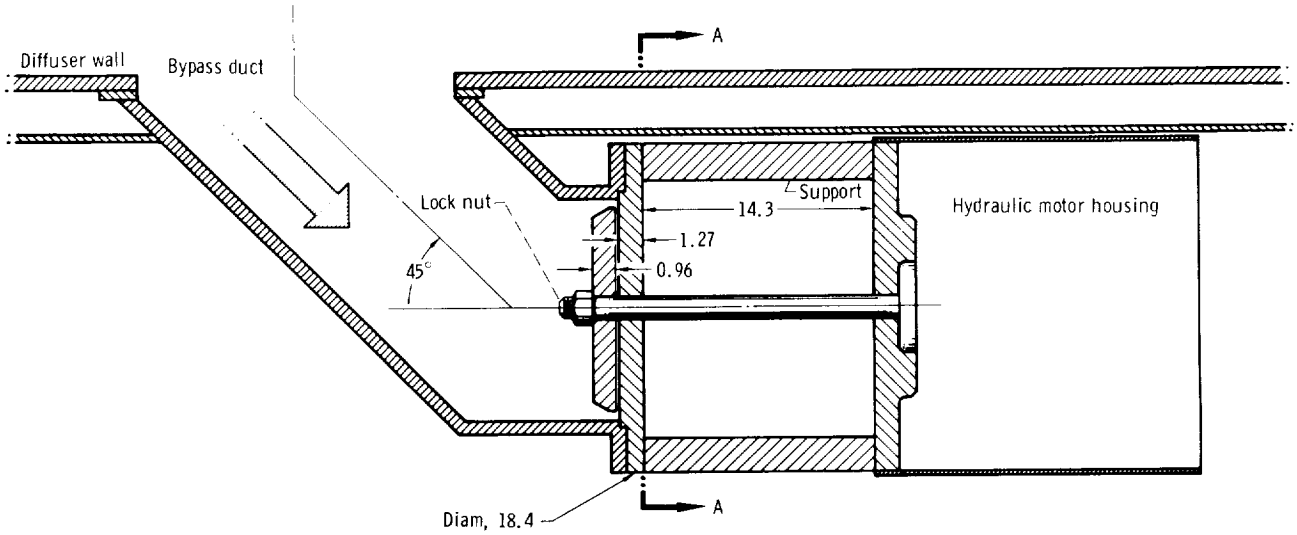

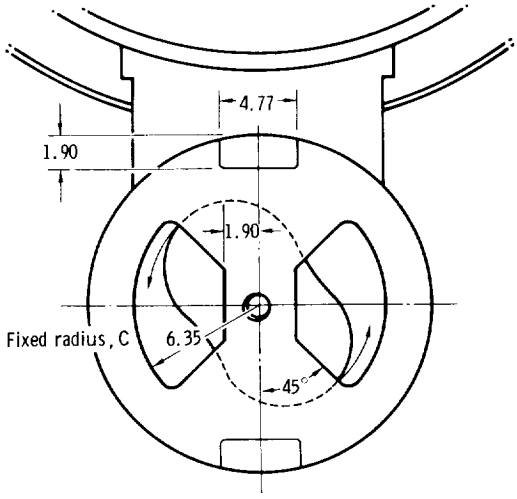

Section A-A

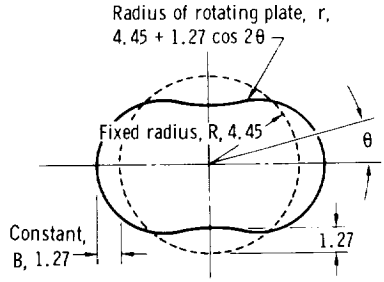

Valve contour

CD-9823-01

Figure 3. - Details of sinusoidal bypass valve and mounting apparatus. (All dimensions are in cm.)

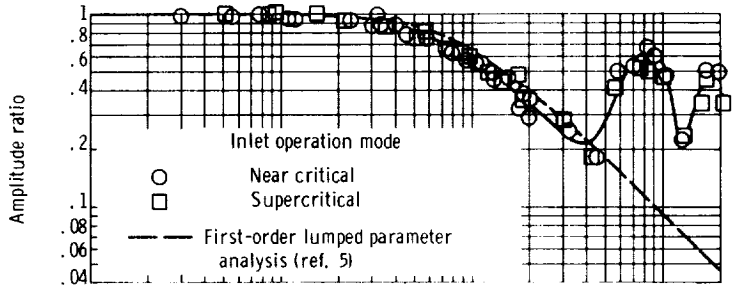

(a) Amplitude ratio.

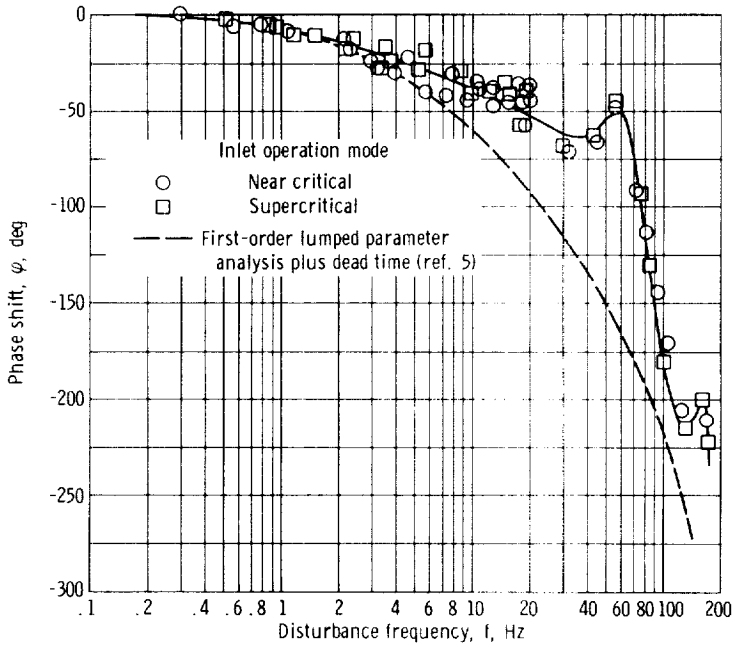

(b) Phase shift.

Figure 10. - Dynamic response of static pressure near inlet throat to internal disturbance.

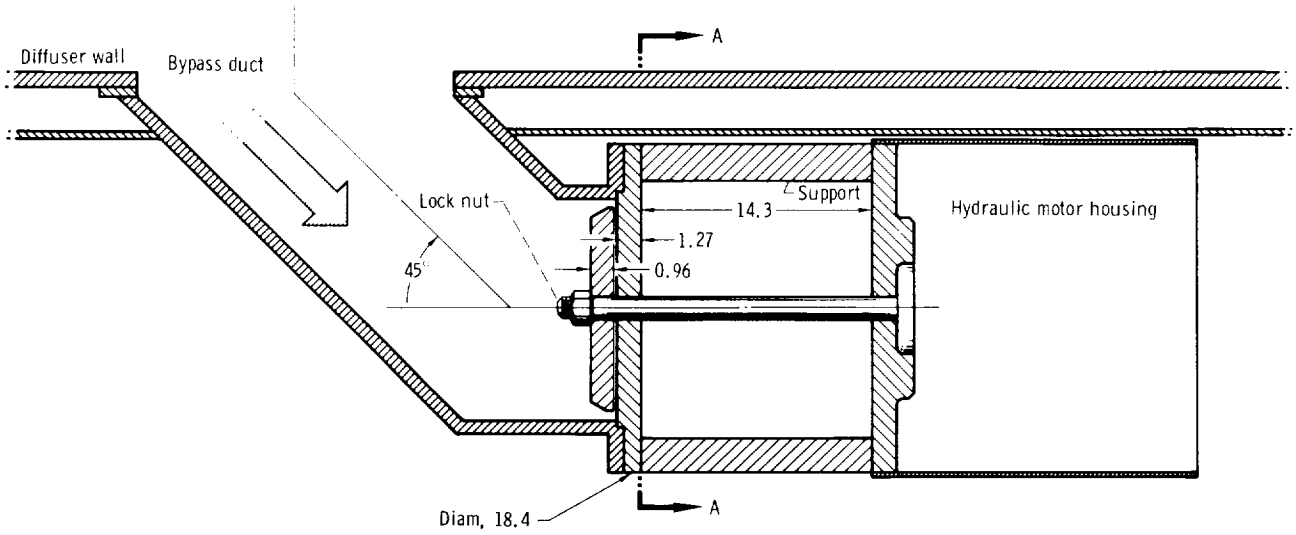

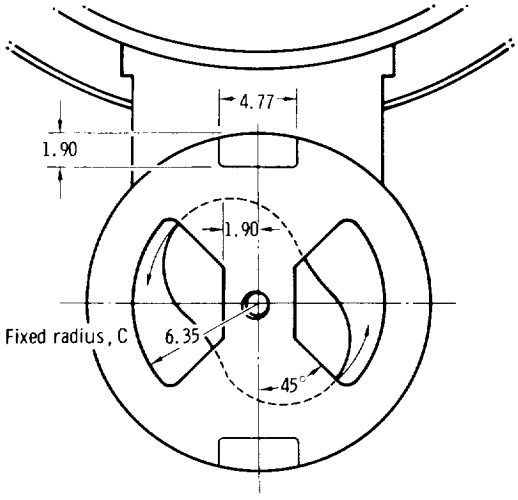

Section A-A

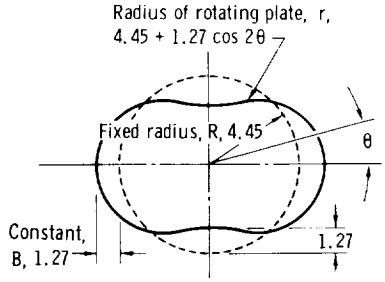

Valve contour

CD-9823-01

Figure 3. - Details of sinusoidal bypass valve and mounting apparatus. (All dimensions are in cm.)

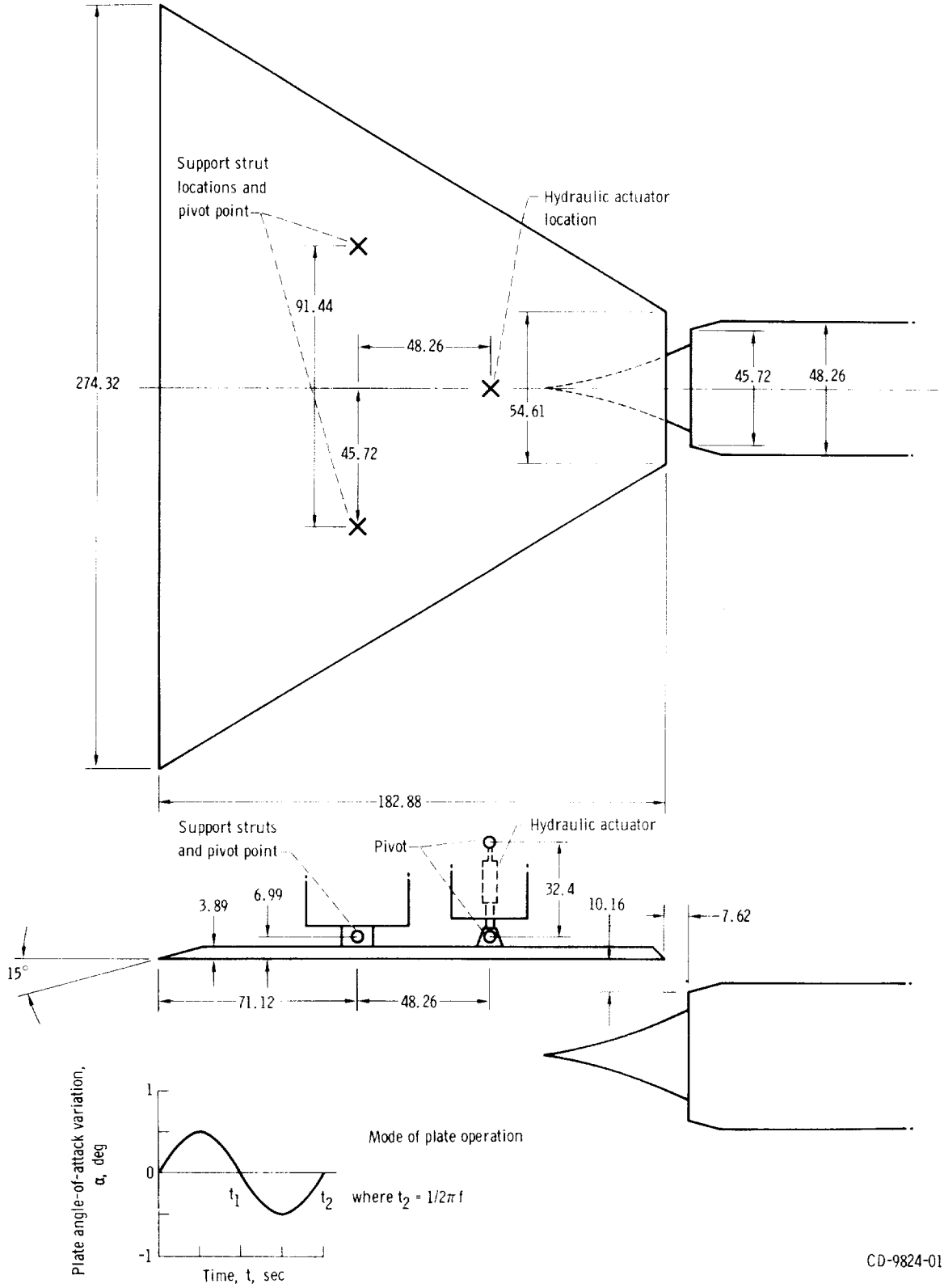

Figure 4. - Details of gust-generator plate and location relative to model. (All dimensions are in cm.)

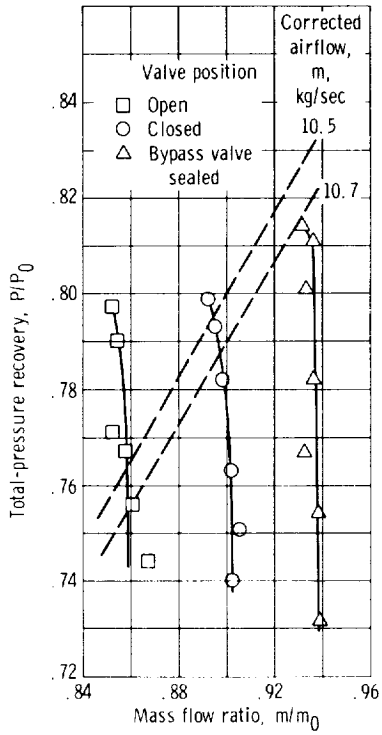

Figure 5. - Inlet operating conditions for rotary-valve sinusoidal area disturbances.

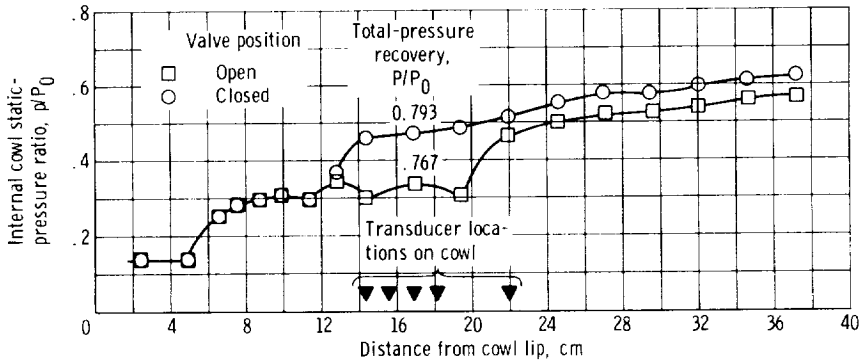

Figure 6. - Effect of valve position on cowl pressure distributions for near-critical operation.

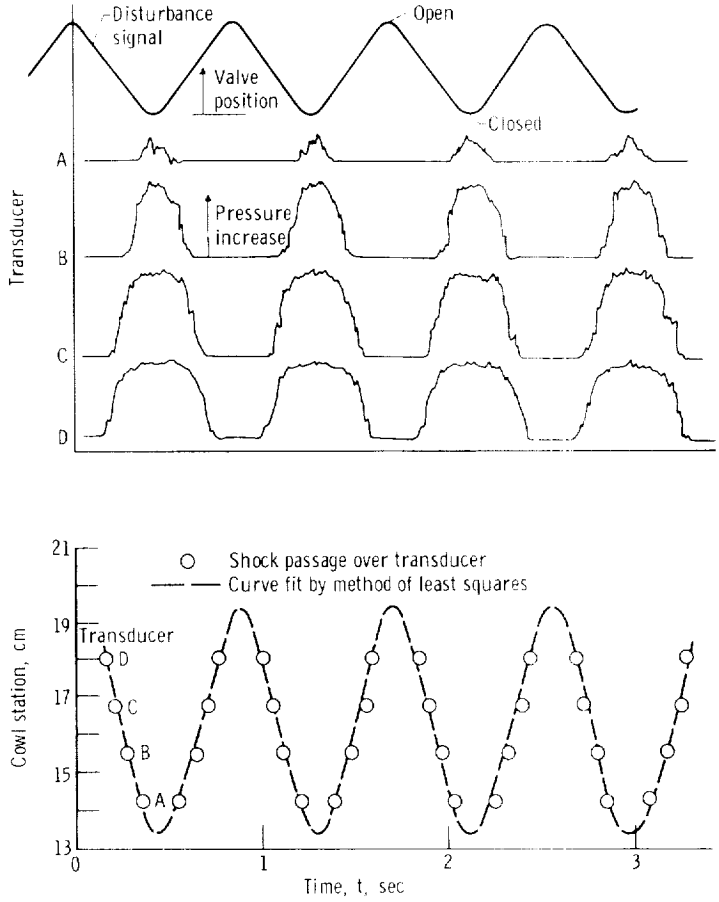

Figure 7. - Data traces and reduction technique for shock position dynamics.

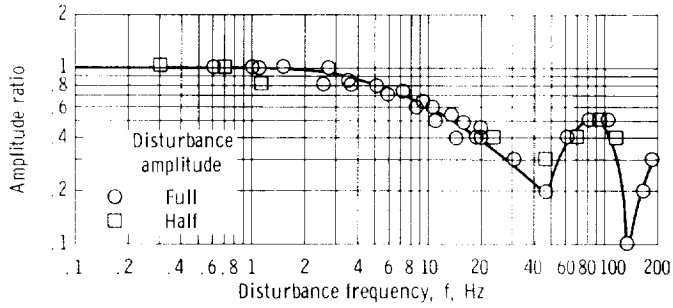

Figure 8. - Terminal shock-position dynamic response to internal disturbance by inlet unstart method.

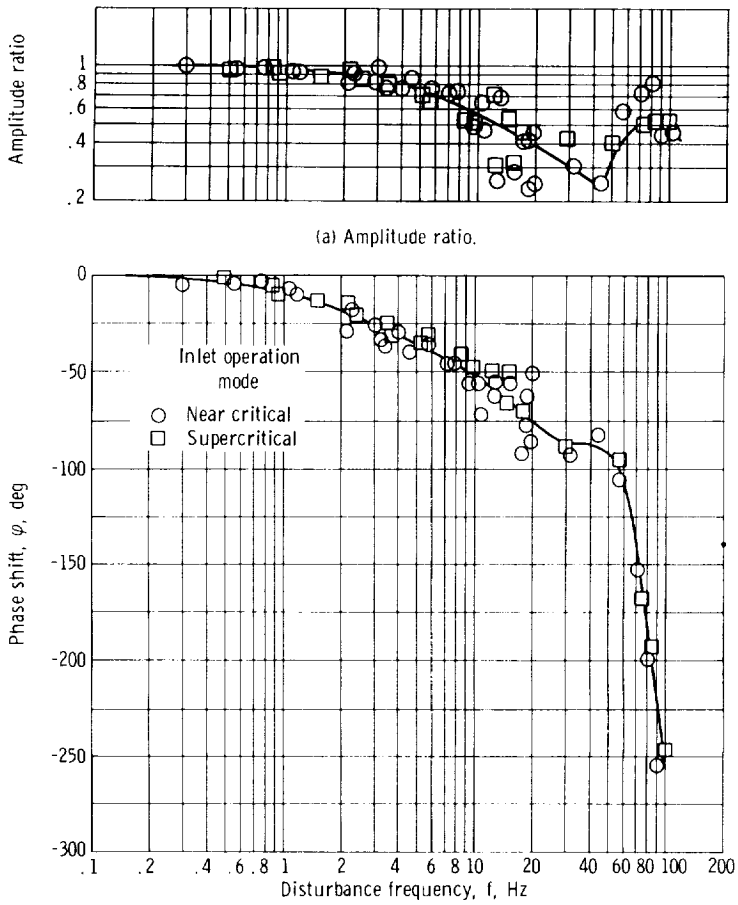

(a) Amplitude ratio.

(b) Phase shift.

Figure 9. - Dynamic response of terminal shock position to internal disturbance.

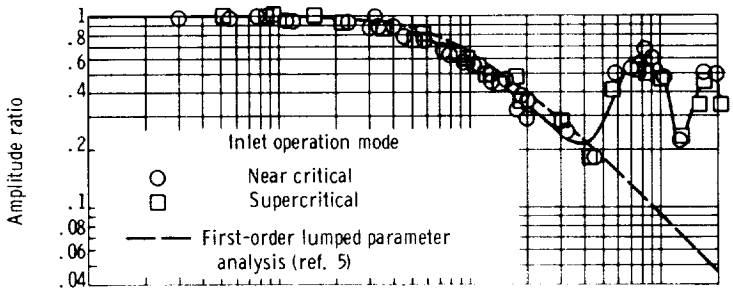

(a) Amplitude ratio.

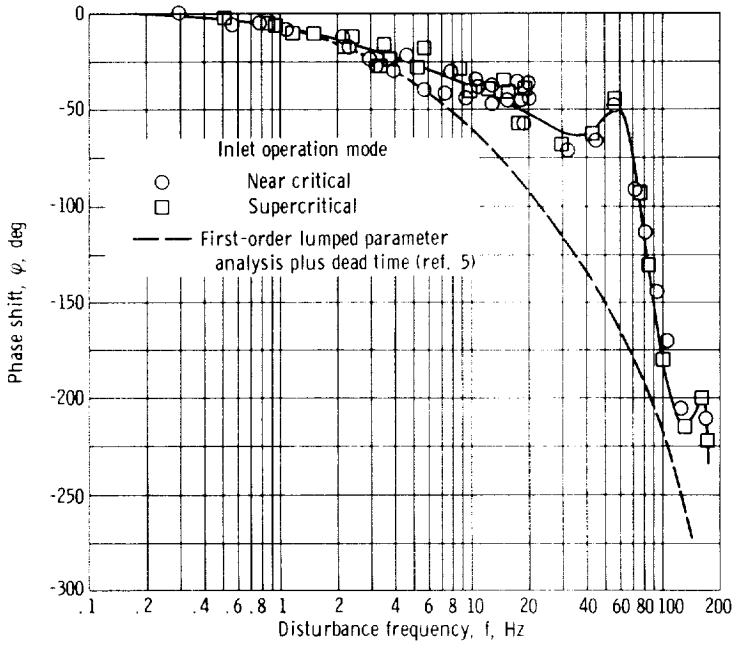

(b) Phase shift.

Figure 10. - Dynamic response of static pressure near inlet throat to internal disturbance.

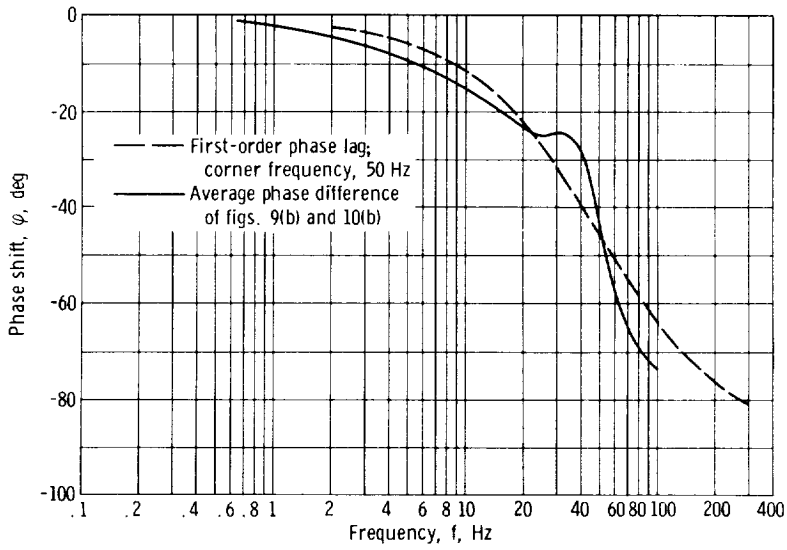

Figure 11. - Phase relation between static-pressure response near inlet throat and terminal shock response for internal disturbance.

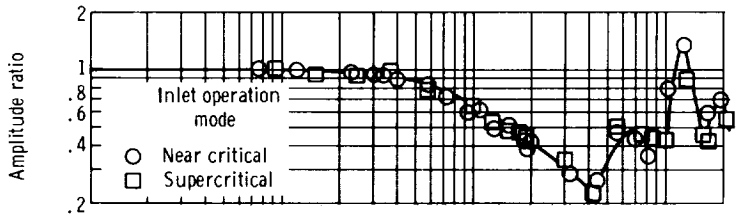

(a) Amplitude ratio.

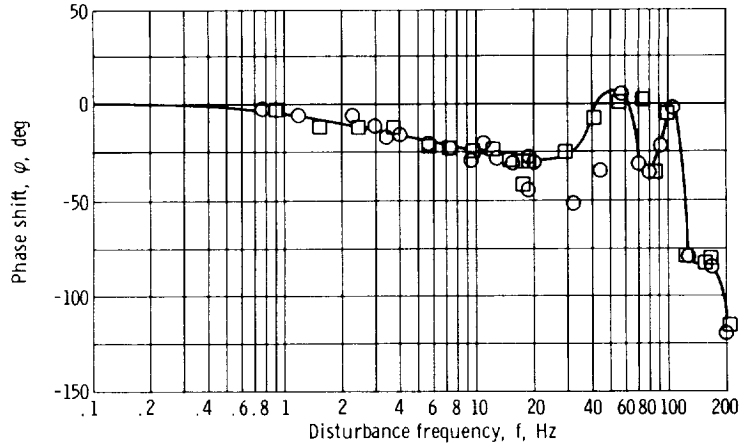

(b) Phase shift.

Figure 12. - Dynamic response of static pressure at diffuser exit to internal disturbance.

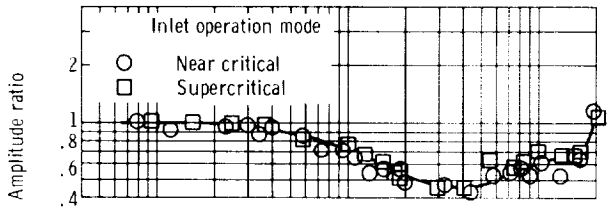

(a) Amplitude ratio.

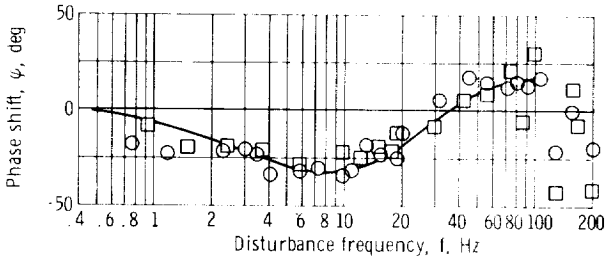

(b) Phase shift.

Figure 13. - Dynamic response of static pressure in bypass duct to internal disturbance.

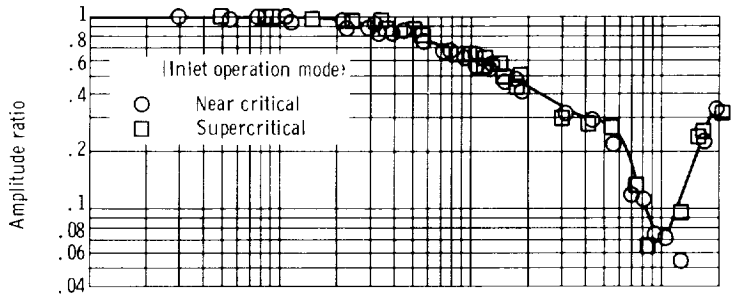

(a) Amplitude ratio.

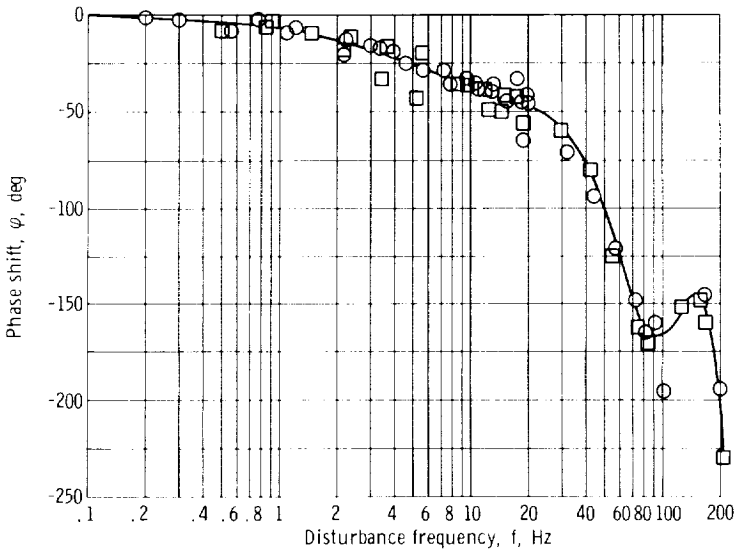

(b) Phase shift.

Figure 14. - Dynamic response of static pressure near model exit to internal disturbance.

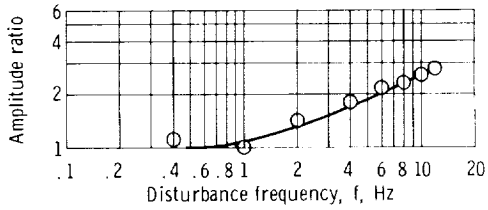

Figure 15. - Terminal shock-position dynamic response by inlet unstart method for external disturbance.

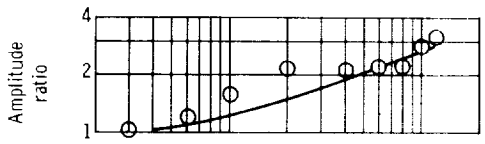

(a) Amplitude ratio.

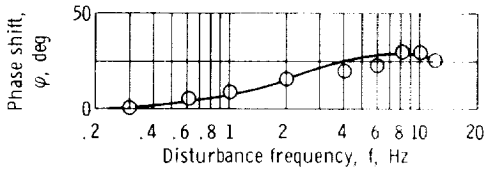

(b) Phase shift.

Figure 16. - Terminal shock-position dynamic response to external disturbance.

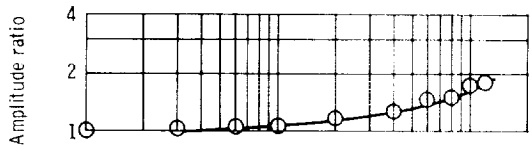

(a) Amplitude ratio.

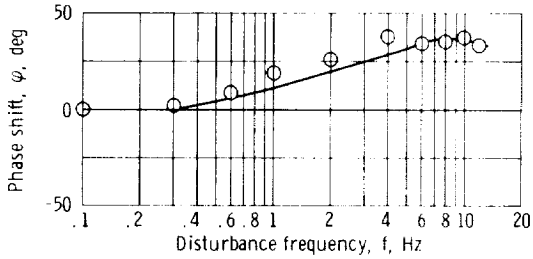

(b) Phase shift.

Figure 17. - Dynamic response of static pressure near inlet throat to external disturbance.